Available online at www.sciencedirect.com
SCIENCE DIRECT®
PERGAMON
International Journal of Multiphase Flow 29 (2003) 1017–1038
International Journal of Multiphase Flow
www.elsevier.com/locate/ijmulflow

Direct numerical simulation of particle wall transfer and deposition in upward turbulent pipe flow

Cristian Marchioli [a], Andrea Giusti [a], Maria Vittoria Salvetti [b], Alfredo Soldati [a,*]

[a] *Dipartimento di Energetica e Macchine, Centro Interdipartimentale di Fluidodinamica e Idraulica, Università degli Studi di Udine, 33100 Udine, Italy*
[b] *Dipartimento di Ingegneria Aerospaziale, Università degli Studi di Pisa, 56100 Pisa, Italy*

Received 25 December 2002; received in revised form 19 February 2003

Abstract

Transfer and deposition of inertial particles or droplets in turbulent pipe flow are crucial processes in a number of industrial and environmental applications. In this work, we use direct numerical simulation (DNS) and Lagrangian tracking to study turbulent transfer and deposition of inertial particles in vertical upward circular pipe flow. Our objects are: (i) to quantify turbulent transfer of heavy particles to the wall and away from the wall; (ii) to examine the connection between particle transfer mechanisms and turbulence structure in the boundary layer. We use a finite difference DNS to compute the three-dimensional time dependent turbulent flow field ($Re_\tau = 337$) and Lagrangian tracking of a dilute dispersion of heavy particles—flyashes in air—to simulate the dynamics of particles. Drag, lift and gravity are used in the equation of motion for the particles, which are assumed to have no influence on the flow field. Particle interaction with the wall is fully elastic. Results on preferential distribution of particles in the boundary layer, particle fluxes to and off the wall and particle deposition mechanisms are shown. Our findings confirm: (i) the specific tendency of particles to segregate in the near-wall region; (ii) the crucial role of the instantaneous realizations of the Reynolds stresses in determining particle fluxes toward and away from the wall; (iii) the relative importance of free-flight and diffusion deposition mechanisms.

* Corresponding author. Tel.: +39-432-558020; fax: +39-432-558803.
E-mail address: soldati@uniud.it (A. Soldati).

0301-9322/03/$ - see front matter
doi:10.1016/S0301-9322(03)00036-3

1. Introduction

The physics of inertial particle transfer in turbulent bounded flows is a phenomenon of great importance in a variety of environmental and industrial processes. Some examples are design and optimization of particle separation devices, solid particulate deposition in combustion and post-combustion devices, microparticle behavior and treatment in smoke exhaust systems and droplet deposition in annular dispersed two-phase flow.

In all of these applications, the fundamental quantities are particle transfer and deposition in the wall-normal direction which are due to complex mechanisms involving coupled interactions between turbulence structures and dispersed phase. Previous results show that particle deposition is controlled by the sweep/ejection cycle, that is by the instantaneous realizations of the Reynolds stresses. Specifically, as suggested by Cleaver and Yates (1975), particles entrained in a sweep, i.e. fluid downwash toward the wall, are expected to approach the wall and, possibly, to contact the boundary, whereas particles entrained in ejections, i.e. outward fluid motions, will be driven away from the wall region into the outer region. The efficiency of these transfer mechanisms is conditioned by the presence of particles available to be transferred, and theoretical (Young and Leeming, 1997; Cerbelli et al., 2001), experimental (Kaftori et al., 1995a,b) and numerical results (McLaughlin, 1989; Ounis et al., 1993) show that transfer to the wall is more efficient than transfer away from the wall.

Previous research has shown that sweep/ejection events are controlled by quasi-streamwise coherent vortices which populate the near-wall region. These vortical structures, which play a fundamental role in the wall turbulence regeneration cycle (Brooke and Hanratty, 1993; Schoppa and Hussain, 1997; Jimenez and Pinelli, 1999; Adrian et al., 2000), are also expected to determine particle transfer fluxes toward and away from the wall.

Owing to the simpler geometry, most of the detailed analyses examining particle transfer in connection with turbulence wall structure have been performed in plane channel flow (Ounis et al., 1993; Kaftori et al., 1995a,b; Pan and Banerjee, 1996; van Haarlem et al., 1998). From a engineering viewpoint, however, particle interaction with turbulence in circular pipe flow is probably more important. Yet, to our knowledge, only Uijttewaal and Oliemans (1996) employed direct numerical simulation (DNS) and Lagrangian tracking to investigate the behavior of inertial particles in a vertical turbulent pipe flow. The authors showed that the particle relaxation time, τ_p, strongly affects the mechanisms of particle motion and deposition in the near-wall region. When τ_p is larger than the integral time scale of near-wall turbulence structures, τ_f, particles are less sensitive to the small time scale of turbulence fluctuations occurring in the near-wall region of the pipe and their behavior is mostly influenced by the overall turbulence characteristics. When τ_p becomes comparable to τ_f, particles can easily follow the large scale motions which characterize the core region of the pipe and become more sensitive to the near-wall turbulence structures. The authors concluded that the interaction between particles and turbulence controls particle segregation in the near-wall layer (turbophoretic drift).

It is known that flows in cylindrical geometries show effects different from those observed in geometries with a rectangular cross-section at the same Re_τ. Such effects have been showed in terms of flow statistics and have been explained, where possible, in terms of a different flow geometry (Eggels et al., 1994; Orlandi and Fatica, 1997). It was also demonstrated that the mean flow properties for pipe flow do not differ from those for channel flow within a distance of roughly

30 wall units from the boundary (Eggels et al., 1994), the position at which turbulence statistics scaled on inner variables become Reynolds-number dependent (den Toonder and Nieuwstadt, 1997). Turning our attention to particles, Uijttewaal and Oliemans (1996) observed that near-wall phenomena as particle near-wall build-up and particle segregation in the low-speed streaks have the same appearance both in pipe flow and in channel flow geometry. Thus, from a qualitative viewpoint, we can safely hypothesize that the near-wall flow features in the two different geometries are similar and that similar physical models can be used to describe particle dynamics very close to the wall.

However, in low-Reynolds number flows, the boundary layer extends up to large fractions of the pipe radius. Specifically, for $Re_\tau \simeq 300$, which is the current standpoint for DNS in circular pipe flows (Eggels et al., 1994; Uijttewaal and Oliemans, 1996; Orlandi and Fatica, 1997), near-wall coherent structures extend up to about 80–100 wall units and reach beyond half the pipe radius. Thus, even though particle transfer to the wall is dominated by near-wall coherent structures, particle fluxes from the core region of the pipe to the wall region may be influenced by the curvature effect.

Starting from this background, in the present paper we report results from a detailed DNS of the passive transport of different size particles in a fully developed upward turbulent flow in a vertical pipe.

The object of this work is to investigate the mechanisms which govern particle transfer, segregation and deposition in vertical pipe. We will provide accurate particle statistics to quantify particle distribution in the boundary layer, particle deposition rates and particle transfer fluxes to the wall and away from the wall. To this aim, we exploited a simulation methodology similar to that used by Uijttewaal and Oliemans (1996) and we tried to improve the accuracy of the current standpoint by tracking larger swarms of particles: we used $O(10^5)$ particles for each particle relaxation time, whereas Uijttewaal and Oliemans (1996) used $O(10^4)$ particles. From a computational viewpoint, the Lagrangian tracking procedure is also different from that adopted by Uijttewaal and Oliemans (1996): since the DNS code solves for the Navier–Stokes equations in a cylindrical domain, we solved particle dynamics in cylindrical coordinates as well.

In this paper, we will also provide new insights into the physical link between particle transfer mechanisms and turbulence structures in the light of previous results obtained for plane channel flow (Marchioli and Soldati, 2002).

In our simulation, we neglected Brownian diffusion, significant for smaller particles, and we assumed a fully elastic particle interaction with the wall. Furthermore, we considered a one-way coupling between particles and flow field, corresponding to the hypothesis of a small loading fraction of the dispersed phase, which does not alter significantly the dynamics of the continuous phase. Since our calculations involved large swarms of particles, the one-way coupling condition reduces the computational effort required, maintaining the general validity of our results. Even though the segregation process can produce local high-particle concentrations near the wall, previous works (Kulick et al., 1994; Kaftori et al., 1995a,b; Pan and Banerjee, 1996) show that turbulence structures seem to modify only from a quantitative viewpoint—small modifications of the intensities (Kulick et al., 1994; Kaftori et al., 1995a,b; Pan and Banerjee, 1996).

This paper is organized as follows: in Section 2, we briefly summarize the details of the DNS code used to compute the turbulent flow field and of the Lagrangian particle tracker. In Section 3, the most important results obtained in our simulations are shown, including the statistics of

particle concentration, particle drift and particle fluxes to the wall. In the final Section, conclusions will be drawn.

2. Numerical simulation

We exploited a DNS database for computing detailed statistics of inertial particles transported by the turbulent carrier flow (hereon referred to as gas).

2.1. Flow field

We simulated a turbulent pipe flow with $Re = \overline{u}D/\nu_g = 4900$ (Orlandi and Fatica, 1997), where $\overline{u}$ is the average velocity, D is the pipe diameter, and ν_g is the fluid kinematic viscosity (the subscript g stands for "gas"). The shear Reynolds number is $Re_\tau = u_\tau D/\nu_g = 337$. The shear velocity u_τ is defined as

$$u_\tau = \sqrt{\frac{\tau_w}{\rho_g}}, \tag{1}$$

where τ_w is shear stress at the wall and ρ_g is gas density. In our simulations, u_τ is equal to 0.1057 m/s.

The DNS code is based on a numerical method developed by Verzicco and Orlandi (1996) (For a comprehensive description of numerical scheme and code implentation the reader is referred to the book by Orlandi, 2000). The spatial discretization of the Navier–Stokes equations is performed by centered finite differences, second-order accurate. The advancement in time is carried by a fractional-step method and a third-order low-storage Runge–Kutta scheme is used for the non-linear terms in the momentum equations in combination with an implicit Crank–Nicolson treatment of the viscous terms. The Navier–Stokes equations are solved in a cylindrical domain (length L, radius R, coordinates θ, r, z) in the transformed variables $q_{g,\theta} = rv_\theta$, $q_{g,r} = rv_r$, and $q_{g,z} = v_z$. Variables are made non-dimensional by using outer units (identified by the superscript "–"), i.e. by taking $\delta_* = R$ and $t^* = R/\overline{u}$ as reference length and time. In the following, however, we will refer to wall units (identified by the superscript "+"), which take $\delta_* = \nu_g/u_\tau$ and $t^* = \nu_g/u_\tau^2$ as reference length and time.

Periodic boundary conditions at the inlet and outlet sections are imposed while the average pressure drop along the pipe length is continuously updated to maintain the mass flowrate constant. No-slip condition is imposed at the pipe wall.

The aspect ratio of the pipe was set to the value $L/R = 10$. This value ensures that correlations along the axial direction decay asymptotically to zero within half of the domain length. Spatial discretization was generated by introducing $N_\theta \times N_r \times N_z = 65 \times 65 \times 65$ grid points in the intervals $[0 : 2\pi]$, $[0 : R]$, $[0 : L]$ spanned by the independent variables θ, r and z (see Fig. 1). Points were equally spaced in the z and θ directions, while a non-uniform discretization was used for the radial coordinate, in order to obtain a finer grid next to the wall (Orlandi and Fatica, 1997). The gridspacing along the axial direction is $\Delta z^+ = 25.84$; the gridspacing along the circumferential direction varies linearly with r from a minimum value $(r\Delta\theta)^+ = 0.056$ near the centerline of the pipe to a maximum value $(r\Delta\theta)^+ = 16.5$ at the pipe wall. The first collocation point away from the

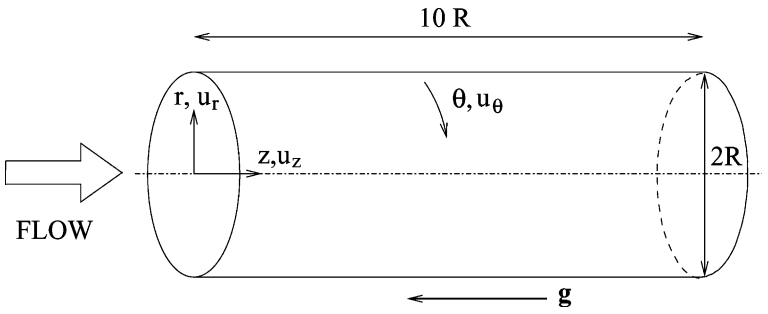

Fig. 1. Diagram of simulated upward pipe flow configuration.

wall is at $r^+ = 0.57$, which yields a grid resolution sufficient to describe the significant length scales in pipe flow, the Kolmogorov length scale being of the order of 1 wall unit.

The initial condition was a (perturbed) Poiseulle flow. The time step, imposed by numerical stability requirements (i.e., to maintain the Courant number below unity), was $\Delta t^+ = 0.115$, which is approximately equal to $10^{-2}\tau_K$, τ_K being the Kolmogorov time scale of fluctuations based on the volume-averaged viscous dissipation.

The simulation was run until the statistics of both average axial velocity and root mean square (RMS) profiles of azimuthal, radial and axial velocity fluctuations were found to be in agreement with those reported in the literature (Eggels et al., 1994). This resulted in $O(10^5)$ time steps, corresponding to $t^+ = 11\,500$.

2.2. Lagrangian particle tracking

Lagrangian particle tracking is used to reproduce the physical situation of solid flyashes entrained by a turbulent flow of air within a vertical pipe and is based upon the detailed knowledge of the fluctuating gas flow field.

Particles and gas densities were set to $\rho_p = 1000$ Kg/m^3 and $\rho_g = 1.3$ Kg/m^3 respectively, while a value $\nu_g = 1.57 \times 10^{-5}$ m^2/s was assumed for the kinematic viscosity of the gas. Three values for particle diameter were considered, namely $d_p = 40$, 120 and 240 μm, corresponding to particle relaxation time of $\tau_p = 4.5 \times 10^{-3}$; 39.2×10^{-3}; 157×10^{-3} s, where $\tau_p = \rho_p d_p^2/18\rho_g\nu_g$ based on Stokes drag law. Data are summarized in Table 1.

Since particles move in a cylindrical domain and the velocity field is calculated in cylindrical coordinates, we calculated the motion of particles in cylindrical coordinates as well. Even though

Table 1
Parameters relative to simulation of particle dispersion

τ_p (ms)	τ_p^+	d_p (μm)	d_p^+
4.5	3.2	40	0.269
39.2	27.9	120	0.808
157	111.6	240	1.616

Superscript '+' identifies non-dimensional variables.

there are published results (Eggels et al., 1994; Orlandi and Fatica, 1997) for the solution of turbulent pipe flow in a cylindrical domain, we found no previous work in the literature reporting on Lagrangian particle tracking in cylindrical coordinates.

The dynamics of the particle is governed by the following set of non-dimensional vectorial equations:

$$\begin{cases} \dfrac{\mathrm{d}\mathbf{x}_\mathrm{p}^+}{\mathrm{d}t^+} = \mathbf{v}_\mathrm{p}^+, \\ \dfrac{\mathrm{d}\mathbf{v}_\mathrm{p}^+}{\mathrm{d}t^+} = \mathbf{f}^+, \end{cases} \tag{2}$$

where $\mathbf{x}_\mathrm{p}^+$ is the particle position, $\mathbf{v}_\mathrm{p}^+$ is the particle velocity and $\mathbf{f}^+$ is the overall force exerted by the gas on the particles. In our simulations, we considered:

$$\mathbf{f}^+ = \mathbf{f}_\mathrm{D}^+ + \mathbf{f}_\mathrm{B}^+ + \mathbf{f}_\mathrm{S}^+ = \frac{\mathbf{F}_\mathrm{D}^+}{m_\mathrm{p}^+} + \frac{\mathbf{F}_\mathrm{B}^+}{m_\mathrm{p}^+} + \frac{\mathbf{F}_\mathrm{S}^+}{m_\mathrm{p}^+}, \tag{3}$$

where m_p^+ is the particle mass and $\mathbf{f}_\mathrm{D}^+$, $\mathbf{f}_\mathrm{B}^+$ and $\mathbf{f}_\mathrm{S}^+$ represent drag, buoyancy and Saffman lift, respectively. The lift force term is written according to Saffman (1965):

$$f_\mathrm{S}^+ = -\xi(\epsilon)\frac{6.46}{6\pi}\frac{a_\mathrm{p}^+}{\tau_\mathrm{p}^+}\left|\frac{\partial u_z^+}{\partial r^+}\right|^{0.5}\mathrm{sign}\left(\frac{\partial u_z^+}{\partial r^+}\right)(v_z^+ - u_z^+), \tag{4}$$

where $\xi(\epsilon)$ is an additional correction factor (always positive) that becomes important when the relative velocity between the particle and the gas is large (McLaughlin, 1991). Wall effects on Saffman lift force are not taken into account in the present paper. Thus, the actual influence of the lift force on particle behavior might be slightly overestimated, specifically for the smaller inertia particles (Wang et al., 1997).

Even if drag force and gravity force are the most effective in determining particle dynamics when $\rho_\mathrm{p} \gg \rho_\mathrm{g}$, Saffman lift due to velocity gradient becomes non-negligible in the proximity of the wall. In turbulent pipe flows, the axial velocity gradient along the radial direction ($\partial u_z^+/\partial r^+$) is the most important and thus the induced Saffman lift is assumed to act in the radial direction only.

Referring to the current case of particles heavier than the carrier fluid and considering an upward flow with negative mean velocity gradient, Saffman lift pushes particles away from the wall when their axial velocity is lower than that of the fluid and pushes particles toward the wall when their axial velocity is greater than that of the fluid.

In this problem, the axial direction (z) is decoupled from the radial (r) and the azimuthal (θ) directions. In cylindrical coordinates, the LHS of Eq. (2) can be rewritten as

$$\frac{\mathrm{d}\mathbf{v}^+}{\mathrm{d}t^+} = \frac{\mathrm{d}}{\mathrm{d}t^+}(v_\theta^+\hat{\mathbf{e}}_\theta + v_\mathrm{r}^+\hat{\mathbf{e}}_\mathrm{r}) = \frac{\mathrm{d}v_\theta^+}{\mathrm{d}t^+}\hat{\mathbf{e}}_\theta + v_\theta^+\frac{\mathrm{d}\hat{\mathbf{e}}_\theta}{\mathrm{d}t^+} + \frac{\mathrm{d}v_\mathrm{r}^+}{\mathrm{d}t^+}\hat{\mathbf{e}}_\mathrm{r} + v_\mathrm{r}^+\frac{\mathrm{d}\hat{\mathbf{e}}_\mathrm{r}}{\mathrm{d}t^+}, \tag{5}$$

where $\hat{\mathbf{e}}_\theta$ and $\hat{\mathbf{e}}_\mathrm{r}$ are the unit vectors of the polar coordinate system. The time derivative of $\hat{\mathbf{e}}_\theta$ and $\hat{\mathbf{e}}_\mathrm{r}$ is not zero since the coordinate system is non-inertial. The rotation velocity of the unit vectors with respect to a cartesian reference system having the same origin can be defined as $\omega^+ = v_\theta^+/r^+$ and the time derivatives of the unit vectors are:

$$\begin{cases} \dfrac{\mathrm{d}\hat{\mathbf{e}}_\theta}{\mathrm{d}t^+} = -\omega^+ \hat{\mathbf{e}}_\mathrm{r} = -\dfrac{v_\theta^+}{r^+}\hat{\mathbf{e}}_\mathrm{r}, \\ \dfrac{\mathrm{d}\hat{\mathbf{e}}_\mathrm{r}}{\mathrm{d}t^+} = \omega^+ \hat{\mathbf{e}}_\theta = \dfrac{v_\theta^+}{r^+}\hat{\mathbf{e}}_\theta. \end{cases} \tag{6}$$

Reworking Eqs. (2), (5) and (6), the two-component (r and θ) equation for particle dynamics becomes:

$$\begin{cases} \dfrac{\mathrm{d}v_\theta^+}{\mathrm{d}t^+} = f_\theta^+ - \dfrac{v_\theta^+ v_\mathrm{r}^+}{r^+}, \\ \dfrac{\mathrm{d}v_\mathrm{r}^+}{\mathrm{d}t^+} = f_\mathrm{r}^+ + \dfrac{v_\theta^{+2}}{r^+}, \end{cases} \tag{7}$$

where f_θ^+ and f_r^+ are the azimuthal and radial components of the external forces acting on the particle respectively, $(v_\theta^+ v_\mathrm{r}^+)/r^+$ is the force arising from the conservation of the angular momentum and v_θ^{+2}/r^+ is the centrifugal force.

Thus, the complete set of non-dimensional scalar equations for the particle motion is:

$$\begin{cases} \dfrac{\mathrm{d}\theta}{\mathrm{d}t^+} = \dfrac{v_\theta^+}{r^+}, \\ \dfrac{\mathrm{d}r^+}{\mathrm{d}t^+} = v_\mathrm{r}^+, \\ \dfrac{\mathrm{d}z^+}{\mathrm{d}t^+} = v_z^+, \\ \dfrac{\mathrm{d}v_\theta^+}{\mathrm{d}t^+} = \dfrac{Cd^+}{\tau_\mathrm{p}^+}(u_\theta^+ - v_\theta^+) + \left(1 - \dfrac{\rho_\mathrm{g}}{\rho_\mathrm{p}}\right) g_\theta^+ - \dfrac{v_\theta^+ v_\mathrm{r}^+}{r^+}, \\ \dfrac{\mathrm{d}v_\mathrm{r}^+}{\mathrm{d}t^+} = \dfrac{Cd^+}{\tau_\mathrm{p}^+}(u_\mathrm{r}^+ - v_\mathrm{r}^+) + \left(1 - \dfrac{\rho_\mathrm{g}}{\rho_\mathrm{p}}\right) g_\mathrm{r}^+ + \dfrac{v_\theta^{+2}}{r^+}, \\ \qquad -\xi(\epsilon)\dfrac{6.46}{6\pi}\dfrac{a_\mathrm{p}^+}{\tau_\mathrm{p}^+}\left|\dfrac{\partial u_z^+}{\partial r^+}\right|^{0.5}\mathrm{sign}\left(\dfrac{\partial u_z^+}{\partial r^+}\right)(v_z^+ - u_z^+), \\ \dfrac{\mathrm{d}v_z^+}{\mathrm{d}t^+} = \dfrac{Cd^+}{\tau_\mathrm{p}^+}(u_z^+ - v_z^+) + \left(1 - \dfrac{\rho_g}{\rho_\mathrm{p}}\right) g_z^+. \end{cases} \tag{8}$$

Owing to the geometry of the pipe, the solution of Eq. (8) has a singularity in the center of the reference system, where the pipe radius r^+ goes to zero. To overcome this problem, the particle equations of motion were written in transformed variables following a procedure similar to that adopted by Verzicco and Orlandi (1996) and by Orlandi and Fatica (1997) to solve the Navier–Stokes equations. The independent variables were chosen as $Q_\theta^+ = (r\theta)^+$, r^+ and z^+, with Q_θ^+ being the auxiliary coordinate for particle position in the azimuthal direction. The dependent variables were defined as $q_\theta^+ = r^+ v_\theta^+$, $q_\mathrm{r}^+ = r^+ v_\mathrm{r}^+$, and $q_z^+ = v_z^+$.

With this choice, the particle momentum balance equation becomes:

$$\begin{cases} \dfrac{\mathrm{d}Q_\theta^+}{\mathrm{d}t^+} = \dfrac{q_\mathrm{r}^+ Q_\theta^+}{r^{+^2}} + \dfrac{q_\theta^+}{r^+}, \\ \dfrac{\mathrm{d}r^+}{\mathrm{d}t^+} = \dfrac{q_\mathrm{r}^+}{r^+}, \\ \dfrac{\mathrm{d}z^+}{\mathrm{d}t^+} = q_z^+, \\ \dfrac{\mathrm{d}q_\theta^+}{\mathrm{d}t^+} = \dfrac{Cd^+}{\tau_\mathrm{p}^+}(q_{f_\theta}^+ - q_\theta^+) + \left(1 - \dfrac{\rho_\mathrm{g}}{\rho_\mathrm{p}}\right) g_\theta^+ r^+, \\ \dfrac{\mathrm{d}q_\mathrm{r}^+}{\mathrm{d}t^+} = \dfrac{Cd^+}{\tau_\mathrm{p}^+}(q_{f_\mathrm{r}}^+ - q_\mathrm{r}^+) + \left(1 - \dfrac{\rho_\mathrm{g}}{\rho_\mathrm{p}}\right) g_\mathrm{r}^+ r^+ + \dfrac{q_\mathrm{r}^{+^2} + q_\theta^{+^2}}{r^{+^2}}, \\ \qquad -\xi(\epsilon)\dfrac{6.46}{6\pi}\dfrac{a_\mathrm{p}^+}{\tau_\mathrm{p}^+}\left|\dfrac{\partial u_z^+}{\partial r^+}\right|^{0.5} \mathrm{sign}\left(\dfrac{\partial u_z^+}{\partial r^+}\right)(q_z^+ - q_{f_z}^+), \\ \dfrac{\mathrm{d}q_z^+}{\mathrm{d}t^+} = \dfrac{Cd^+}{\tau_\mathrm{p}^+}(q_{f_z}^+ - q_z^+) + (1 - \dfrac{\rho_g}{\rho_\mathrm{p}}) g_z^+, \end{cases} \tag{9}$$

where $C_\mathrm{d}^+ = C_\mathrm{d}/C_\mathrm{S}$ is the ratio between the effective drag coefficient $C_\mathrm{d} = 24/Re_\mathrm{p} + 0.44$ and the Stokes drag coefficient $C_\mathrm{S} = 24/Re_\mathrm{p}$.

To understand the physics of turbulent dispersion in the most simplified setting, other forces acting on the particle, such as hydrostatic force, Magnus effect, added mass force and Basset history force, have been neglected in writing Eq. (9), their contribution being orders of magnitude smaller than that of the effects considered (Armenio and Fiorotto, 2001).

Working with the transformed variables q_θ^+, q_r^+ and q_z^+ allows: (i) to overcome the problem that the value of v_θ^+ and v_r^+ at the axis is undetermined because of the numerical scheme used to solve the DNS simulation, and (ii) to reduce the stiffness of the system at the pipe axis ($r^+ = 0$) with respect to canonical cylindrical coordinates. To track particles in the discretized DNS flow field, the nodal values of q_θ^+, q_r^+ and q_z^+ were computed by using a trilinear interpolation scheme in cylindrical coordinates. Time-efficient low-order interpolation schemes proved to be accurate enough to maintain statistical accuracy (van Haarlem et al., 1998) and to preserve local resolution for the small scales of the boundary layer (Rouson and Eaton, 2001).

Eq. (9) was solved by using a fifth-order adaptive size Runge–Kutta scheme, assuming a time piecewise constant velocity field of the gas phase. In other words, the gas flow field was considered "frozen" within each time interval of the DNS simulation. This approximation is justified by the fact that the DNS time-step is much smaller than both the Kolmogorov time scale of fluctuations based on the volume averaged viscous dissipation, τ_K, and the particle relaxation time (in wall units, it results $\Delta t_\mathrm{DNS}^+ \sim [10^{-2}\text{–}10^{-1}]\tau_\mathrm{p}^+$, depending on particle diameter).

Particle tracking simulations were run for 10^4 time-steps, corresponding to $t^+ = 1150$. This time interval is long enough to obtain reliable results on deposition rates and other Eulerian statistics.

We assumed gravity acting along the axis of the pipe with the mean flow of the carrier fluid directed upward, driven by a pressure gradient (see Fig. 1). The initial condition was generated by injecting the flow domain with $\mathrm{O}(10^5)$ randomly distributed particles, whose initial velocity was set equal to the interpolated fluid velocity at the particle position. Particles that came closer than one particle radius from the boundary were elastically reflected away from the wall. Particles

exiting the outlet section were assumed to re-enter the inlet section instantaneously, according to the periodic boundary condition of the DNS simulation.

3. Results and discussion

In this section we show results relevant to analyze turbulent particle dispersion, deposition and segregation in the near-wall region of a cylindrical vertical pipe. For brevity, we do not show the statistics of the flow field, since the numerical code we used in our simulations was validated previously for pipe flows (Orlandi and Fatica, 1997). We do not show the statistics of particle motion either, since they just confirm the expected particle behavior with respect to the carrier fluid and do not add to previous works (Uijttewaal and Oliemans, 1996).

3.1. Particle distribution in the boundary layer

In Fig. 2, the instantaneous top view of particle distribution for all particle sets is shown at different times of the simulation. For clarity of presentation, we show only a pipe length of about 300 wall units before the outlet. At time $t^+ = 0$, particles are uniformly distributed in the computational domain.

From Fig. 2a–c, it is apparent that the distribution of $\tau_p^+ = 3.2$ particles hardly changes during the initial transient of about $1000t^+$: due to their small relaxation time, these particles behave approximately as fluid tracers and need longer times to modify their initial uniform distribution.

A different behavior is found for both $\tau_p^+ = 27.9$ particles and $\tau_p^+ = 111.6$ particles. At time $t^+ = 695$ (Fig. 2e and h), the near-wall build-up of particles develops. This behavior has been reported in several previous works (Kallio and Reeks, 1989; Young and Hanratty, 1991; Chen and McLaughlin, 1995; Uijttewaal and Oliemans, 1996). Fig. 2f and i, taken at $t^+ = 1150$, show more clearly the non-random fashion of particle clustering. In particular, the black circles indicate particle clusters that approach the walls through preferential avenues and strike the wall.

Focusing on Fig. 2i, we observe large void regions indicating the presence of a large streamwise vortex. Due to the small Reynolds number of the flow, these void regions can extend up to more than 80 wall units from the wall, reaching roughly half cylinder radius. No large-scale structure is put in evidence by particle behavior in the core region of the pipe.

In Fig. 3 we show the mean particle concentration for the three particle sets as a function of the radial distance r^+ from pipe axis. Profiles are normalized to the initial particle concentration. Consider that particles of the three dimensions investigated touch the wall at $r^+ = 0.135$, $r^+ = 0.405$ and $r^+ = 0.808$ respectively. Starting from the initial uniform particle distribution, profiles were computed by subdividing the pipe into 400 concentric annular shells of equal volume and counting the fraction of particles that fell within each shell, i.e. by averaging over the axial and the azimuthal directions.

Results show that, for each size particles are non-uniformly distributed along the radial direction. There is an accumulation in the near-wall region, which increases in time, and the concentration profiles appear to reach a maximum very close to the wall (between 1 and 2 wall units from the boundary). It is apparent that $\tau_p^+ = 3.2$ particles slowly transfer to the wall and that $\tau_p^+ = 27.9$ particles transfer to the wall faster than $\tau_p^+ = 111.6$ particles.

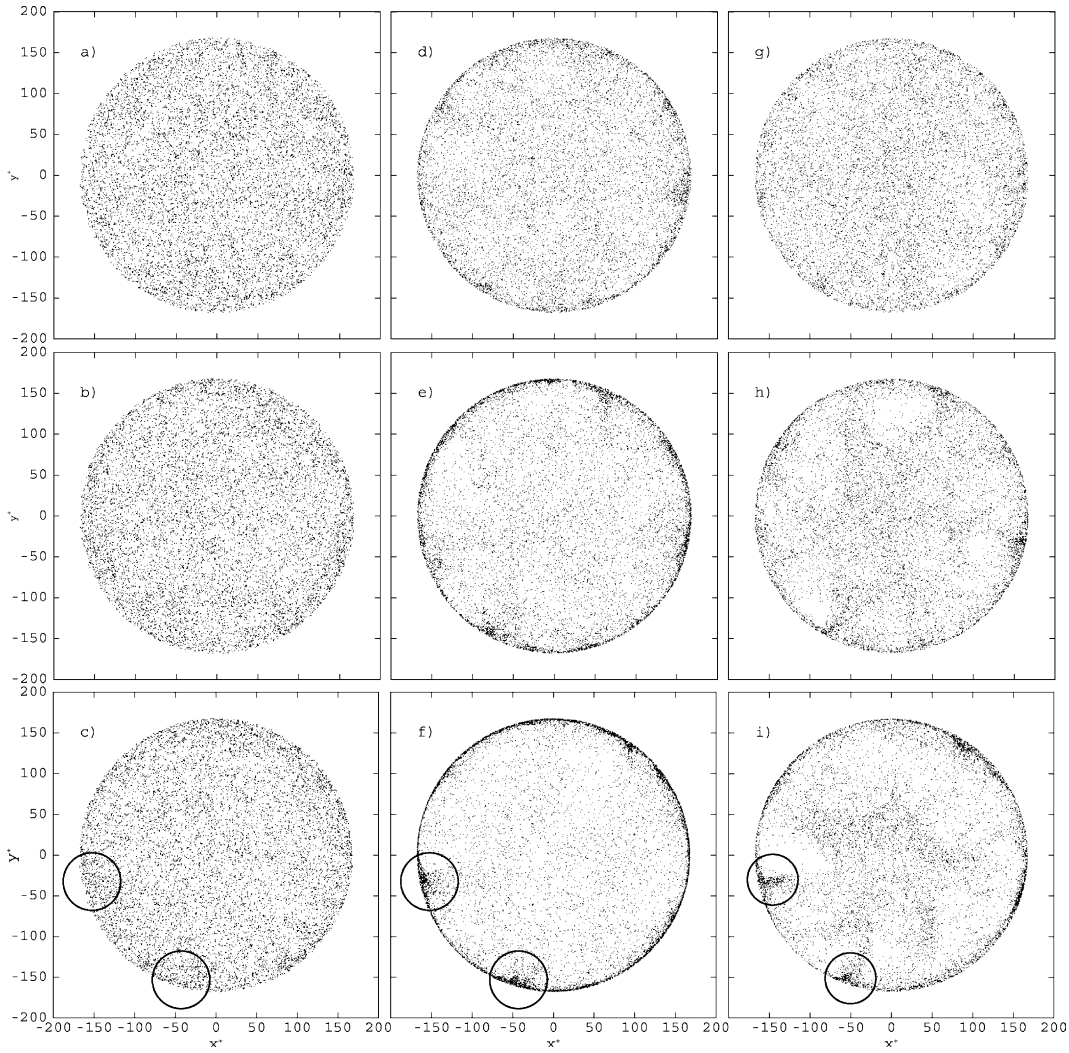

Fig. 2. Top view of particle distribution in pipe flow at different simulation times. (a), (d) and (g): distribution at time $t^+ = 174$ for $\tau_p^+ = 3.2$, $\tau_p^+ = 27.9$, $\tau_p^+ = 111.6$ respectively. (b), (e) and (h): distribution at time $t^+ = 695$ for $\tau_p^+ = 3.2$, $\tau_p^+ = 27.9$, $\tau_p^+ = 111.6$ respectively. (c), (f) and (i): distribution at time $t^+ = 1150$ for $\tau_p^+ = 3.2$, $\tau_p^+ = 27.9$, $\tau_p^+ = 111.6$ respectively.

Particle migration to the wall in turbulent boundary layers is a well-known phenomenon, which is usually referred to as turbophoretic drift (Caporaloni et al., 1975; Reeks, 1983) and is attributed to the non-homogeneous distribution of turbulent velocity fluctuations in the wall-normal direction. We will try to describe the mechanisms leading to turbophoretic drift by elucidating the connection between particle dynamics and the near-wall turbulence structure.

Even when segregated in the viscous sublayer, particles do not attain a uniform distribution in the spanwise direction. It has been shown that, for turbulent flow in a plane channel, particle position tends to correlate with the instantaneous location of the low-speed streaks, defined as

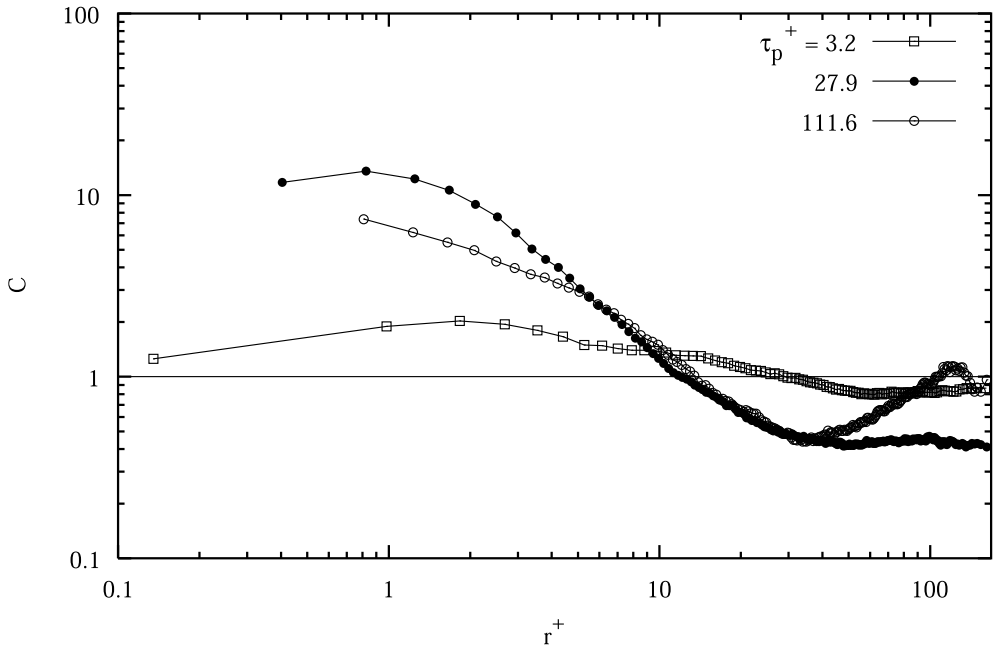

Fig. 3. Number density distribution for $\tau_p^+ = 3.2$, $\tau_p^+ = 27.9$ and $\tau_p^+ = 111.6$ particles at time $t^+ = 1150$.

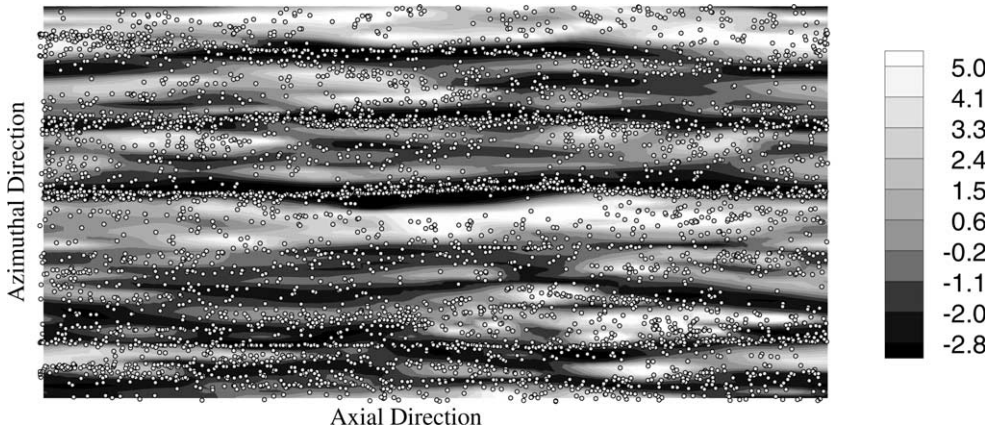

Fig. 4. Preferential concentration of $\tau_p^+ = 27.9$ particles in the low-speed streaks environment (represented by dark regions of negative axial velocity fluctuation u_z' at a distance $r^+ = 5$ from the wall of the pipe). Flow is from left to right.

regions of lower-than-mean streamwise velocity (Kaftori et al., 1995a,b; Pan and Banerjee, 1996; van Haarlem et al., 1998). We find similar results for turbulent flow in a circular pipe. Fig. 4 shows the instantaneous distribution of $\tau_p^+ = 27.9$ particles in the region between the wall and $r^+ = 5$, superimposed onto the contours of the axial velocity fluctuation u_z' on a θ–z plane close to the wall ($r^+ = 5$). Fig. 4 corresponds to the particle concentration profile at time $t^+ = 1150$, shown in Fig. 3. Particles tend to line up along the low-speed streaks, avoiding the high-speed regions.

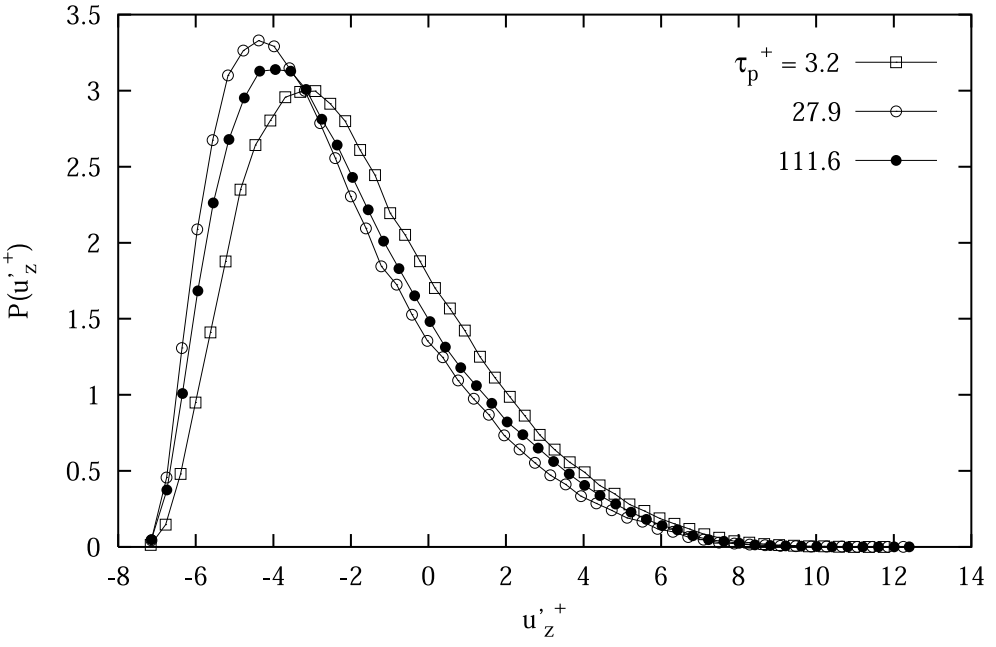

Fig. 5. Correlation between particle number density distribution in the wall region of the pipe with the non-dimensional streamwise fluctuating velocity u_z' for $\tau_p^+ = 3.2$, $\tau_p^+ = 27.9$, $\tau_p^+ = 111.6$ particles.

In Fig. 5 we show the particle number density distribution as a function of the non-dimensional fluctuation of the axial velocity, u_z', in the near-wall region ($5 \leqslant r^+ \leqslant 15$).

We computed the particle number density distribution as follows: (i) we calculated the average axial velocity of the fluid $\overline{u}(r)$ in the region $5 \leqslant r^+ \leqslant 15$, (ii) we subdivided this region in 10 equally spaced slabs, (iii) we determined the slab containing the particle, (iv) we computed the local axial velocity fluctuation of the fluid $u_z'(r,\theta,z) = u_z(r,\theta,z) - \overline{u}(r)$ in the position of the particle, (v) we counted the number of particles associated with each value of $u_z'(r,\theta,z)$ and normalized it by the total number of particles located into each slab.

From Fig. 5, it appears that a clear bias exists between the positive and the negative values of u_z' for each particle set. This indicates that all particles, regardless of their size, tend to concentrate preferentially in the regions of fluid velocity lower than the mean.

3.2. Particle transfer fluxes

The observed particle accumulation in the wall region of the pipe indicates that particle transfer to the wall is more efficient than particle transfer away from the wall. As shown in Fig. 2, particle transfer is achieved through preferential pathways which correspond to strongly coherent advective motions, namely sweeps and ejections. These motions scale with the buffer layer, represent the instantaneous realizations of the Reynolds stresses, and contribute to positive turbulence production. The presence of a sweep corresponds to a local increase of the shear stress at the wall whereas the presence of an ejection corresponds to a local decrease of the shear stress at the wall.

In Fig. 6, we highlight the spatial correlation of the location of sweeps and ejections and the preferential locations where particles penetrate and exit the wall layer. In Fig. 6a, we show the probability density function of sweep/ejection events plotted as a function of the local wall shear stress, which is normalized to its average value. Sweeps and ejections are separated by a crossover level of the wall shear stress: sweeps correspond to high-shear stress regions and ejections correspond to low-shear stress regions. A slight overlapping between the two distributions exists and the value 1.0 of the normalized shear stress separates "high" and "low" shear stress regions.

In Fig. 6b–d, the probability density function of particles having positive wall-normal velocity—toward the wall—and negative wall-normal velocity—toward the outer flow—is plotted as a function of the normalized local wall shear stress. In our simulation, particles do not reach a steady state distribution profile. Thus, we tried to quantify particle fluxes toward the wall and away from the wall by counting the particles having positive or negative wall-normal velocity

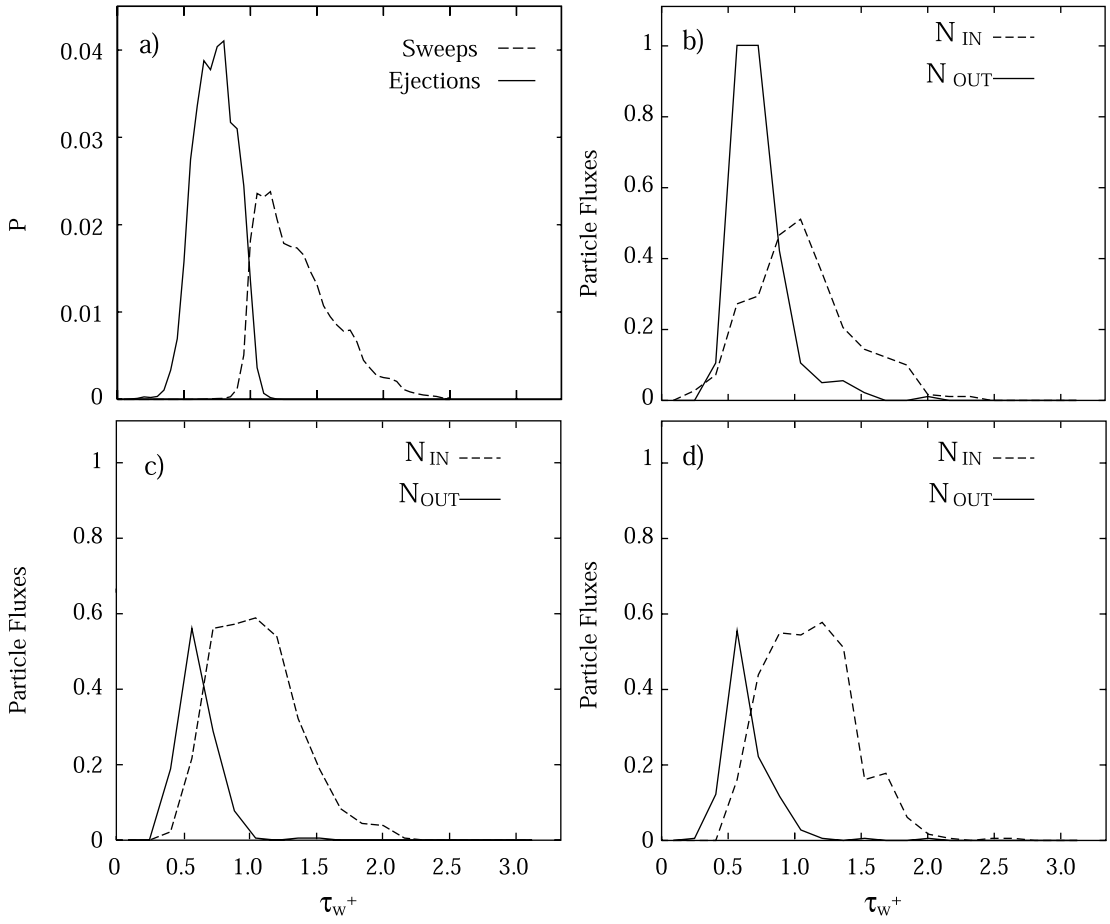

Fig. 6. Correlation between particle fluxes in and out the wall layer and wall shear stress distribution. (a) Probability distribution of sweep/ejection events versus wall shear stress. (b), (c) and (d) Correlation of the normalized particle fluxes in and out the wall layer with (b) $\tau_p^+ = 3.2$, (c) $\tau_p^+ = 27.9$ and (d) $\tau_p^+ = 111.6$ particles.

instantaneously present in a monitor slab of 10 wall units (from $r^+ = 5$ to $r^+ = 15$ from the wall). The profiles reported in Fig. 6b–d were computed from:

$$N_{\mathrm{IN/OUT}} = \frac{\sum_{i=1}^{20} n_i}{TA}, \tag{10}$$

where n_i is the number of particles with negative/positive wall-normal velocity w_p counted at the measuring points per unit time, T is the length of the time averaging period and A is the measuring area (Kaftori et al., 1995b). To have a larger particle set for calculating particle fluxes, we averaged fluxes over a short time interval of length $\Delta t^+ = 5.78$ (20 instantaneous realizations of the flow field). All plots are normalized by the peak value obtained for the $\tau_\mathrm{p}^+ = 3.2$ particles flux toward the outer flow, which appears to be the most intense.

Two main conclusions can be drawn from Fig. 6b–d. First, it is confirmed that, regardless of particle size, a strong correlation exists between particle fluxes to the wall, N_IN, and high-wall shear stress regions, which correspond to sweep events. Low-wall shear stress regions correspond to ejection events and are well correlated with off-the-wall particle fluxes, N_OUT (Marchioli and Soldati, 2002). Second, fluxes to the wall involve a larger number of particles compared with fluxes toward the outer flow, this trend being enhanced when particle size is larger (even for $\tau_\mathrm{p}^+ = 3.2$ particles, the area under the N_IN-curve, representing the overall intensity of particle flux toward the wall, is about 10% larger than the area under the N_OUT-curve, representing the overall intensity of particle flux away from the wall). This confirms that, particularly in the case of high-inertia particles, ejections are somehow unable to lift up all the particles that sweeps drive toward the wall, i.e. particles tend to settle in a sediment layer at the wall, which roughly corresponds to the viscous sublayer.

Transfer mechanisms for circular pipe reported in this section compare well with those obtained for plane channel (Marchioli and Soldati, 2002) and confirm the similarity between the two flow configurations in the vicinity of the wall (Orlandi and Fatica, 1997; den Toonder and Nieuwstadt, 1997). It is also verified that the instantaneous realizations of the Reynolds stresses represent the dominant mechanism by which particles are transferred toward and away from the wall (Marchioli and Soldati, 2002).

3.3. Particle deposition

The turbulent mass transport equation included in the model by Cousins and Hewitt (1968) states that the particle deposition flux J is proportional to particle concentration C and to the area of deposition A_d. The flux J is the rate at which non-interacting particles deposit ($\mathrm{d}N/\mathrm{d}t$) while particle concentration C is defined as the ratio between the number of particles N and the occupied volume ϕ (N/ϕ). We can thus write:

$$\frac{\mathrm{d}N}{\mathrm{d}t} = -k_\mathrm{d}\frac{NA_\mathrm{d}}{\phi}, \tag{11}$$

where the deposition coefficient k_d is the constant of proportionality. Given the initial number N_0 of particles released in the pipe and the number N_dep of particles already deposited at a given time t, we discretized the previous quantities as follows:

$$J = \frac{1}{A_d}\frac{dN}{dt} = \frac{\Delta N_{dep}}{\Delta t^+ L^+ 2\pi r^+_{dep}}, \tag{12}$$

$$C = \frac{N}{\phi} = \frac{N_0 - N_{dep}}{L^+ \pi r^+_{dep} 2}, \tag{13}$$

where L^+ is the non-dimensional length of the pipe and r^+_{dep} is the distance from the axis of the pipe at which a particle deposits. Since we assumed that a particle deposits when its center is less than a distance $d^+_p/2$ from the boundary, we obtain $r^+_{dep} = R^+ - d^+_p/2$.

To reproduce the condition of perfectly absorbing wall imposed by Uijttewaal and Oliemans (1996), particles are labelled as deposited even if they are subsequently re-entrained in the core region of the pipe. We identified a fictitious cylindrical surface of radius r^+_{dep} to separate the core region of the pipe from the deposition region. Within this region, we computed J and C from Eqs. (12) and (13) by counting the number of particles ΔN_{dep} deposited during subsequent time intervals Δt^+ equal to three viscous wall time units. Upon substitution of Eqs. (12) and (13) into Eq. (11), we obtain the following expression for the deposition coefficient:

$$k^+_d = \frac{\Delta N_{dep} r^+_{dep}}{2\Delta t^+ (N_0 - N_{dep})}. \tag{14}$$

According to Eq. (14) the deposition coefficient can be obtained from the profiles for the decrease of particle number in time due to deposition (N_{dep}/N_0). In Fig. 7, these profiles are shown in a semi-log plot. After 800 t^+, more than 40% of $\tau^+_p = 27.9$ and $\tau^+_p = 111.6$ particles have deposited. The close-up in Fig. 7 shows that only 0.03% of $\tau^+_p = 3.2$ particles were labelled as deposited during the same time interval.

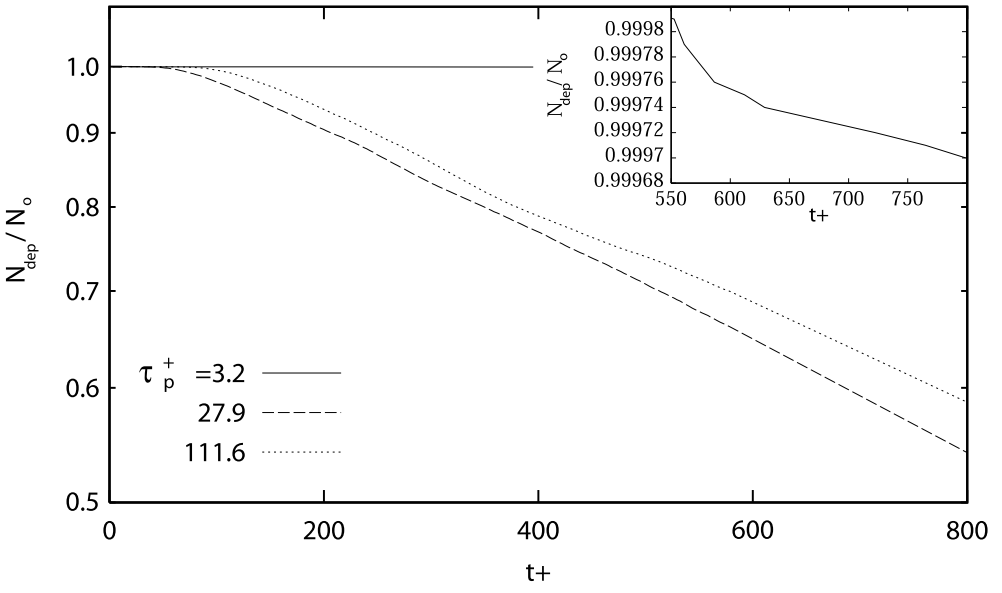

Fig. 7. Decrease of particle number in time due to deposition ($N_0 = 10^5$). For clarity, a close-up of the $\tau^+_p = 3.2$ particles profile from $t^+ = 550$ to $t^+ = 800$ is also shown.

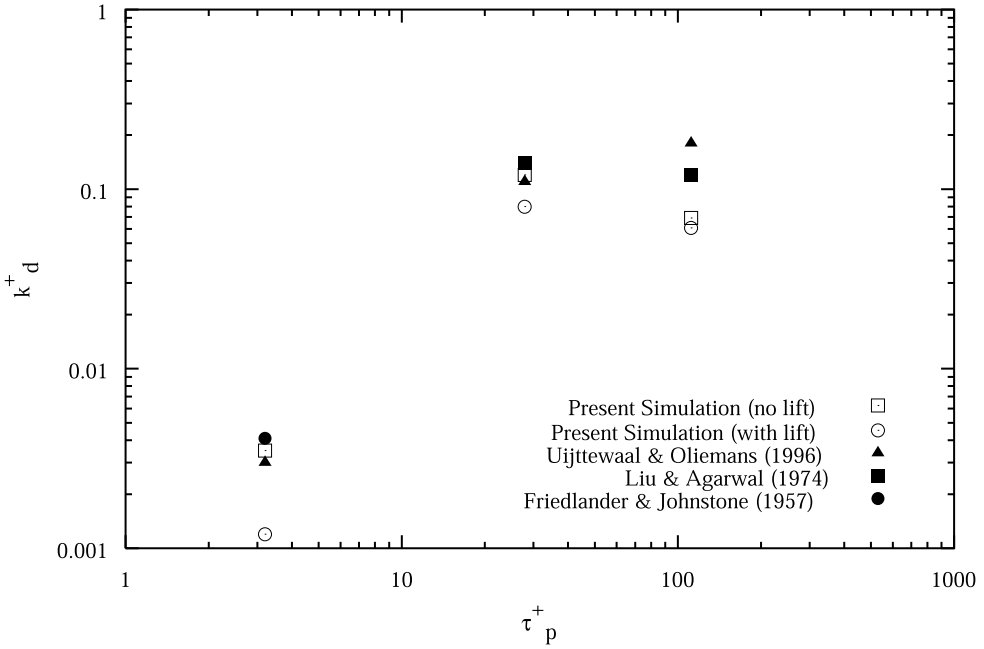

Fig. 8. Deposition coefficients for all particle sets as a function of non-dimensional particle relaxation time τ_p^+.

The slope at the linear part of each profile gives the constant value for k_d^+: note that, depending on particle size, constant deposition rates are attained at different times. In Fig. 8, we show the different values for k_d^+ as a function of particle relaxation time. We present result for the two simulations, without and with the Saffman lift force acting on particles. As previously observed for vertical upward flow, lift decreases particle deposition. This decrease is smaller for larger particles, the deposition of which is controlled by the inertia gained in regions far from the wall.

For comparison, we also show the numerical results obtained by Uijttewaal and Oliemans (1996), who performed a pipe flow simulation at $Re_\tau = 360$, comparable to the present simulation, and tracked $O(10^4)$ particles subject to drag force only. From a qualitative viewpoint, our results show that gravity, not considered by Uijttewaal and Oliemans (1996), contributes to reduce particle deposition. Experimental data on particle deposition in vertical upward pipe flow have been reported by Friedlander and Johnstone (1957) and by Liu and Agarwal (1974). Even though the experimental trend is captured by our simulations, the agreement with our computations is not quantitative. Yet, we should remark here that there is no general consensus among authors on the accurate value of deposition rates (Young and Leeming, 1997).

3.4. Particle deposition mechanisms

By examining Fig. 8, we observe that deposition rates are much larger for particles with larger τ_p^+. It is widely accepted (Friedlander and Johnstone, 1957) that different mechanisms control particle deposition in turbulent bounded flows. Specifically, deposition of large particles ($\tau_p^+ > 200$) is dominated by inertia effect whereas deposition of small particles ($\tau_p^+ < 0.03$) is

dominated by diffusion effects, i.e. the small intensity turbulent fluctuations in proximity of the wall. Particles with intermediate inertia are bound to deposit by either mechanism. In a recent work (Narayanan et al., 2003), deposition mechanisms for intermediate size particles in plane channel flow were examined in detail. It was found that, for particles with $\tau_p^+ = 5$–15, diffusion is the dominant deposition mechanism.

To examine the instantaneous deposition mechanisms in pipe flow, we employed the same method to quantify the time spent by the depositing particle in the near-wall region before deposition. Focusing on a thin slab of fluid close to the wall, three wall units thick, we followed each particle path to the wall and we recorded the time spent before deposition. If a particle escapes the slab before depositing (due to re-entrainment), the time counter for that particle is reset to zero. As in Narayanan et al. (2003), we tried to find a relationship between the particle residence time in the slab and the velocity of the particle at deposition.

In Fig. 9, we show a scatter plot of the non-dimensional particle residence time (T_{res}^+) versus the particle wall-normal deposition velocity (w_{dep}^+) for the three particle sets. We focus first on Fig. 9a–c, which are relative to the simulations with no lift force acting on particles. As expected, high-deposition velocity correlates with short residence time in the monitor slab whereas low-deposition velocity correlates well with short residence times in the monitor slab. We can thus identify

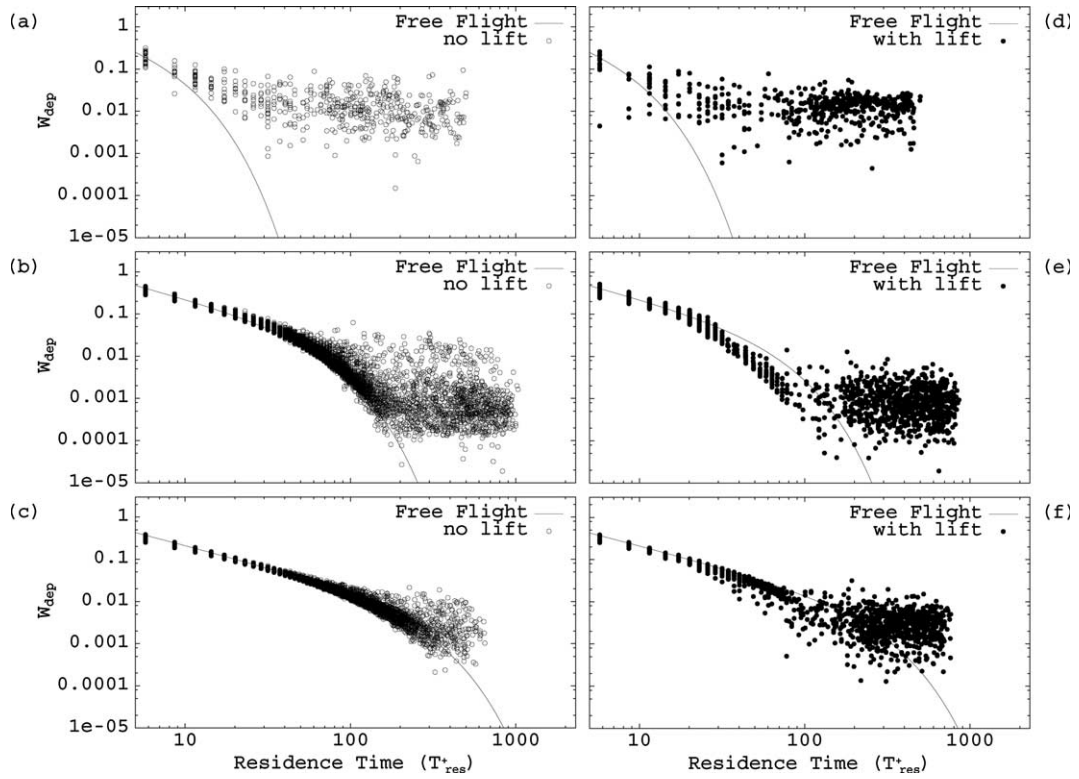

Fig. 9. Residence time of particles in a slab of $z^+ < 3$ versus wall-normal deposition velocity. Pictures (a), (b) and (c): simulations without lift, pictures (d), (e) and (f): effect of Saffman lift. Particle relaxation times: (a) and (d): $\tau_p^+ = 3.2$; (b) and (e): $\tau_p^+ = 27.9$; (c) and (f): $\tau_p^+ = 111.6$.

two distinct populations: the *free-flight* particles and the *diffusional deposition* particles (Narayanan et al., 2003). While free-flight particle velocities are larger than the near-wall fluid velocity fluctuations, diffusional deposition particles have velocity roughly equal to the near-wall fluid velocity fluctuations (Narayanan et al., 2003). Observing Fig. 9a, diffusional deposition appears to be the dominant mechanism of deposition for small particle relaxation times.

Focusing on a near-wall region where the wall-normal fluid velocity fluctuations are negligible with respect to the wall-normal particle velocity ($z^+ < 3$ for the residence time analysis), the free-flight deposition mechanism can be predicted by the following ballistic equation (Narayanan et al., 2003):

$$\frac{\mathrm{d}w_\mathrm{p}^+}{\mathrm{d}t} = -\frac{w_\mathrm{p}^+}{\tau_\mathrm{p}^+}, \tag{15}$$

in which we consider only the motion in the wall normal direction. Solving Eq. (15) for a particle controlled by the Stokes drag, entering the monitor slab with wall-normal velocity $w_\mathrm{p}^+(z^+ = 3)$ at time $t^+ = 0$ and depositing with wall-normal velocity $w_\mathrm{dep}^+ = w_\mathrm{p}^+(z^+ = d_\mathrm{p}^+/2)$ at time T_res^+, we can find the following relationship between T_res^+ and w_dep^+:

$$\tau_\mathrm{p}^+ w_\mathrm{dep}^+ \left[1 - \exp\left(\frac{T_\mathrm{res}^+}{\tau_\mathrm{p}^+}\right)\right] = 3 - d_\mathrm{p}^+/2, \tag{16}$$

where $3 - d_\mathrm{p}^+/2$ on the right-hand side is the actual slab height chosen for the residence time analysis (Narayanan et al., 2003). We plotted Eq. (16) in Fig. 9. Apparently, Eq. (16) predicts well the behavior of particle depositing with large velocity and largerly underpredicts deposition times for particles depositing by diffusion mechanism. Small particles (Fig. 9a) deposit almost exclusively by diffusion, whereas for large particles free-flight deposition is dominant.

In an attempt to compute the relative extent of the two populations, we define V_f as the volume fraction of particles depositing by free-flight and $V_\mathrm{D} = 1 - V_\mathrm{f}$ as the volume fraction of particles depositing by diffusion. Considering a particle depositing by free-flight mechanism only, if its behavior differs from Eq. (16) by no more than 10%, then about 95% of $\tau_\mathrm{p}^+ = 3.2$ particles deposit by diffusion, about 60% of $\tau_\mathrm{p}^+ = 27.9$ particles deposit by diffusion and about 10% of $\tau_\mathrm{p}^+ = 111.6$ particles deposit by diffusion. This by no means implies that free-flight particles are less well correlated with the fluid motions. Almost all particles are brought in the vicinity of the wall by sweeps: once there, particle trajectory curvature (i.e., particle momentum) becomes important in determining the dominant deposition mechanism.

We can examine the influence of the lift force on particle deposition velocity in Fig. 9d–f. Lift force appears to reduce the deposition velocity for particles depositing by free-flight, whereas the diffusion deposition mechanism appears to be influenced only for smaller particles. As from Eq. (4), the lift force depends on the relative axial velocity between the dispersed phase and the carrier phase. In Fig. 10 the axial mean velocity profiles for fluid and particles are plotted. Due to gravity, particles move slower than the fluid—close to the wall they actually fall down—so that in the average the lift force is directed from the wall toward the pipe axis in the entire domain, thus explaining Figs. 8 and 9. As discussed previously, the lift force equation used in the present work does not account for wall effects.

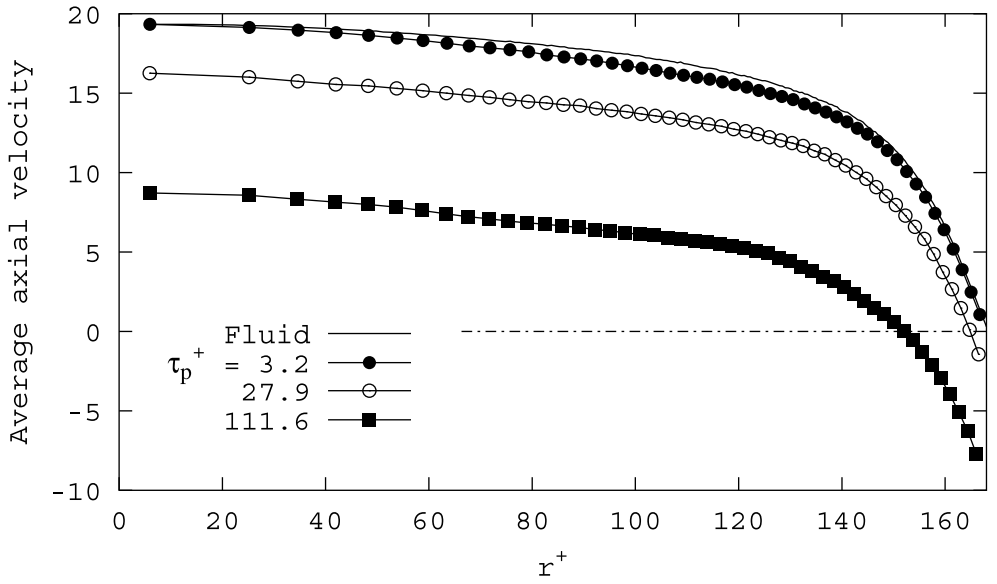

Fig. 10. Average axial velocity profiles.

Wang et al. (1997) employed a large eddy simulation to verify an optimal equation for the lift force which considered the wall effect. They also demonstrate that the wall effect reduces the lift correction. Applying the observations by Wang et al. (1997) to our flow field and to the range of particles we examined, we found that the wall effects may play a role beyond $y^+ = 2$ for $\tau_p^+ = 111.6$ particles, beyond $y^+ = 3$ for $\tau_p^+ = 27.9$ particles and beyond $y^+ = 5$ for $\tau_p^+ = 3.2$ particles. The quantitative influence of this effect is to be investigated in a separate work and we will limit here our analysis to the qualitative influence of the lift force.

From Fig. 9, diffusional deposition and free-flight deposition appear competing mechanism and act in parallel also for large particles. From a practical engineering viewpoint, this observation is crucial and should lead to develop deposition models capable of accounting for both mechanisms acting in parallel. A model of the type we developed in a previous paper (Soldati and Andreussi, 1996), in which the overall deposition coefficient is given by

$$k_d = V_F k_d^F + (1 - V_F) k_d^D, \tag{17}$$

should ensure a more accurate prediction of deposition rates. DNS data could be used to evaluate the volume fractions, the free-flight deposition coefficient k_d^F, and the diffusion deposition coefficient k_d^D.

4. Summary and conclusions

Prediction of accurate transfer and deposition rates in turbulent pipe flows is crucial for several industrial and environmental applications. Yet, due to the simpler geometry, most of the DNS including particle dynamics refer to plane channel flow and only Uijttewaal and Oliemans (1996)

studied particle dispersion in pipe flow. Their study, however, was focused more on the influence of the pipe Reynolds number and particles were subject to drag force only.

In this paper, we quantified turbulent transfer, segregation and deposition of heavy particles to the wall and away from the wall in vertical upward pipe flow using DNS coupled with Lagrangian tracking of large swarms of particles. A noteworthy computational aspect in the Lagrangian tracking procedure is the use of cylindrical coordinates in connection with a set of proper transformed variables to rewrite the particle motion equations. This choice allows to solve particle dynamics with no need to know the value of azimuthal and radial velocity components at the pipe axis, where the equations have a singularity, and contributes to reduce the stiffness of the system at the axis with respect to canonical cylindrical coordinates.

We also examined the connection between the turbulence structure of the boundary layer and particle transfer and deposition mechanisms. Besides the well-known phenomena of particle clustering and near-wall build-up, a strong correlation exists between sweep/ejection events and particle fluxes in and out the wall layer: strongly coherent sweeps drive particles toward the wall while strongly coherent ejections drive particles toward the outer flow. By calculating the probability that a particle will go toward the wall or away from the wall conditioned by the presence of a sweep or an ejection, we found that these coherent local convective motions are effective in transferring small particles. As the ratio of particle timescale to fluid structure timescale increases, the sweep/ejection cycle becomes less efficient due to particle capability of filtering out the effects of the smaller fluid scales (which characterize the near-wall region).

The balance of transfer mechanisms gives the net fluxes to the wall, which lead to non-uniform distribution of particles both in the spanwise and in the wall-normal directions. In particular, since the tendency of particle concentration to peak very close to the wall might be exploited in a number of applications, e.g. to optimize particle filtering devices in smoke exhaust systems, in an effort to add to previous theories (Caporaloni et al., 1975; Reeks, 1983), we tried to characterize in detail the dynamics of particles entering and exiting the wall layer in connection with the dynamics and the synchronicity of the wall structures. We addressed the problem in the light of previous results observed also for channel flow geometry (Marchioli and Soldati, 2002).

Results on particle transfer fluxes have been correlated with the dominant mechanisms for particle deposition in wall-bounded flows also examining separately the influence of the lift force. Focusing on a tiny slab located well into the viscous sublayer, a clearcut distinction between particle depositing by diffusion and particle depositing by free-flight can be made. For all particle sizes we investigated—$\tau_p^+ = 3.2$, $\tau_p^+ = 27.9$, $\tau_p^+ = 111.6$—we found that: (i) diffusional deposition is the dominant mechanism for $\tau_p^+ = 3.2$ and $\tau_p^+ = 27.9$ particles whereas free-flight deposition is the dominant mechanism for $\tau_p^+ = 111.6$ particles, (ii) as in channel flow case (Narayanan et al., 2003), a single one-dimensional ballistic equation reproduces the free-flight.

To summarize the diffusion deposition mechanism, we can identify the following cycle: (1) a particle is brought in the wall layer by a sweep; once in the wall layer this particle may be: (2a) re-entrained to the outer flow by an ejection or (2b) due to the synchronicity of the sweep/ejection cycle with the dynamics of the near-wall quasi-streamwise coherent vortical structures (see Marchioli and Soldati, 2002 for details), the particle may be trapped in the viscous region; (3) particles are then deposited by the residual turbulence fluctuations of the viscous sublayer (see Narayanan et al., 2003 for details). This scenario is crucial for all approaches aiming at quanti-

fying particle transfer and deposition rates and should be included in practical engineering models for deposition.

Acknowledgements

Financial support from MURST under Grant 9809326392_005 is gratefully acknowledged. Thanks to Professor Paolo Orlandi for providing the computational code and to Stefano Cerbelli for running the DNS.

References

Adrian, R.J., Meinhart, C.D., Tomkins, C.D., 2000. Vortex organization in the outer region of the turbulent boundary layer. J. Fluid Mech. 422, 1–54.

Armenio, V., Fiorotto, V., 2001. The importance of the forces acting on particles in turbulent flows. Phys. Fluids 13, 2437–2440.

Brooke, J.W., Hanratty, T.J., 1993. Origin of turbulence-producing eddies in channel flow. Phys. Fluids A 5, 1011–1022.

Caporaloni, M., Tampieri, F., Trombetti, F., Vittori, O., 1975. Transfer of particles in nonisotropic air turbulence. J. Atmos. Sci. 32, 565–568.

Cerbelli, S., Giusti, A., Soldati, A., 2001. ADE approach to predicting dispersion of heavy particles in wall bounded turbulence. Int. J. Multiphase Flow 27, 1861–1879.

Chen, M.W., McLaughlin, J.B., 1995. A new correlation for the aerosol deposition rate in vertical ducts. J. Colloid Interface Sci. 169, 437–455.

Cleaver, J.W., Yates, B., 1975. A sub layer model for the deposition of particles from a turbulent flow. Chem. Eng. Sci. 30, 983–992.

Cousins, L.B., Hewitt, G.F., 1968. Liquid phase mass transfer in annular two-phase flow. UKAEA Report, AERE-R 5657.

Eggels, J.G.M., Unger, F., Weiss, M.H., Westerwell, J., Adrian, R.J., Friedrich, R., Nieuwstadt, F.T.M., 1994. Fully developed turbulent pipe flow: a comparison between direct numerical simulation and experiment. J. Fluid Mech. 268, 175–209.

Friedlander, S.K., Johnstone, H.F., 1957. Deposition of suspended particles from turbulent gas streams. Ind. Eng. Chem. Res. 49, 1151–1156.

van Haarlem, B., Boersma, B.J., Nieuwstadt, F.T.M., 1998. Direct numerical simulation of particle deposition onto a free-slip and no-slip surface. Phys. Fluids 10, 2608–2620.

Jimenez, J., Pinelli, A., 1999. The autonomous cycle of near-wall turbulence. J. Fluid Mech. 389, 335–359.

Kaftori, D., Hetsroni, G., Banerjee, S., 1995a. Particle behavior in the turbulent boundary layer. I. Motion, deposition, and entrainment. Phys. Fluids 7, 1095–1106.

Kaftori, D., Hetsroni, G., Banerjee, S., 1995b. Particle behavior in the turbulent boundary layer. II. Velocity and distribution profiles. Phys. Fluids 7, 1107–1121.

Kallio, G.A., Reeks, M.W., 1989. A numerical simulation of particle deposition in turbulent boundary layers. Int. J. Multiphase Flow 15, 433–446.

Kulick, J.D., Fessler, J.R., Eaton, J.K., 1994. Particle response and turbulence modification in fully developed channel flow. J. Fluid Mech 277, 109–134.

Liu, B.Y., Agarwal, J.K., 1974. Experimental observation of aerosol deposition in turbulent flow. J. Aerosol Sci. 5, 145–155.

Marchioli, C., Soldati, A., 2002. Mechanisms for particle transfer and segregation in turbulent boundary layer. J. Fluid Mech. 468, 283–315.

McLaughlin, J.B., 1989. Aerosol particle deposition in numerically simulated channel flow. Phys. Fluids A 1, 1211–1224.

McLaughlin, J.B., 1991. Inertial migration of a small sphere in linear shear flows. J. Fluid Mech. 224, 261–274.

Narayanan, C., Lakehal, D., Botto, L., Soldati, A., 2003. Mechanisms of particle deposition in a fully-developed turbulent open channel flow. Phys. Fluids 15, 763–775.

Orlandi, P., 2000. Fluid Flow Phenomena. A Numerical Toolkit. Kluwer Academic Publishers, London.

Orlandi, P., Fatica, M., 1997. Direct simulations of turbulent flow in a pipe rotating about its axis. J. Fluid Mech. 343, 43–72.

Ounis, H., Ahmadi, G., McLaughlin, J.B., 1993. Brownian particle deposition in a directly simulated channel flow. Phys. Fluids A 5, 1427–1432.

Pan, Y., Banerjee, S., 1996. Numerical simulation of particle interactions with wall turbulence. Phys. Fluids 8, 2733–2755.

Reeks, M.W., 1983. The transport of discrete particles in inhomogeneous turbulence. J. Aerosol Sci. 14, 729–739.

Rouson, D.W.I., Eaton, J.K., 2001. On the preferential concentration of solid particles in turbulent channel flow. J. Fluid Mech. 428, 149–169.

Saffman, P.G., 1965. The lift on a small sphere in a slow shear flow. J. Fluid Mech. 22, 385–400, 1968 and Corrigendum 31, 624.

Schoppa, W., Hussain, F., 1997. Genesis and dynamics of coherent structures in near-wall turbulence. In: Panton, R. (Ed.), Self-sustaining Mechanisms of Wall Turbulence. In: Advances in Fluid Mechanics, vol. 15. Computational Mechanics Publications, pp. 385–422.

Soldati, A., Andreussi, P., 1996. The influence of coalescence on droplet transfer in vertical annular flow. Chem. Eng. Sci. 51, 353–363.

den Toonder, J.M.J., Nieuwstadt, F.T.M., 1997. Reynolds number effects in a turbulent pipe flow for low to moderate Re. Phys. Fluids 9, 3398–3409.

Uijttewaal, W.S., Oliemans, R.V.A., 1996. Particle dispersion and deposition in direct numerical and large eddy simulations of vertical pipe flows. Phys. Fluids 8, 2590–2604.

Verzicco, R., Orlandi, P., 1996. A finite-difference scheme for three-dimensional incompressible flows in cylindrical coordinates. J. Comput. Phys. 123, 402–414.

Wang, Q., Squires, K.D., Chen, M., McLaughlin, J.B., 1997. On the role of the lift force in turbulence simulation of particle deposition. Int. J. Multiphase Flow 23, 749–763.

Young, B., Hanratty, T.J., 1991. Trapping of solid particles at a wall in a turbulent flow. AIChE J. 37, 1529–1536.

Young, J., Leeming, A., 1997. A theory of particle deposition in turbulent pipe flow. J. Fluid Mech. 340, 129–159.